Overcoming the Detectability Obstacle in Adaptive Output Feedback Control of DC-DC Boost Converter With Unknown Load

Tavan, Mehdi; Sabahi, Kamel; Hajizadeh, Amin; Soltani, Mohsen N.; Jessen, Kasper

Published in:
IEEE Transactions on Control Systems Technology

DOI (link to publication from Publisher):
10.1109/TCST.2020.3044378

Publication date:
2021

Document Version
Accepted author manuscript, peer reviewed version

Overcoming the Detectability Obstacle in Adaptive Output Feedback Control of DC–DC Boost Converter With Unknown Load

Mehdi Tavan, Kamel Sabahi, *Member, IEEE*, Amin Hajizadeh, *Senior Member, IEEE*, Mohsen N. Soltani, *Senior Member, IEEE*, and Kasper Jessen

***Abstract*— This brief proposes a solution to the long-standing problem of designing an adaptive control for the dc–dc boost converter with unknown load and unavailable input current measurement. The difficulty lies in the parametric uncertainty of the output dynamics, which poses a manifold of equilibria in the classical adaptive observer design. This is known as the *detectability obstacle* that imposes a restrictive assumption on the system behavior to ensure convergence. To overcome this problem, a class of saturated dynamic controllers is designed to guarantee the asymptotic regulation of the output voltage. An *immersion- and invariance*-based adaptive observer is proposed, which preserves the convergence property in conjunction with the controller with no need for an extra *persistent excitation* condition. To evaluate the transient behavior of the proposed controller, realistic simulations are provided, and then the performance comparison with two other well-known output feedback controllers is presented. Moreover, experimental results are concluded on a prototype dc–dc boost converter to support and verify the results of theory and simulations.**

***Index Terms*— Adaptive observer, dc–dc boost converter, detectability obstacle, Lyapunov stability analysis, nonlinear control.**

I. Introduction

ONE of the important applications of Automatic Control theory is the control of power electronic systems. Due to providing some challenging theoretical properties, such as *bilinear*, nonminimum-phase nature with respect to the output to be regulated and *underactuated*-type system with saturated control input, boost converters have attracted the interest of many researchers to evaluate the new control techniques [1]–[3]. Also, the control of this system is currently an active field of research because of its broad applications in Renewable Energy, Smart Grid, Fuel Cell Hybrid Electric Vehicles, Marine Vehicles, and Aerospace Vehicles [4]–[6].

Combining the differential equations, which represent the circuit behavior for a fixed position of switches, suggests a dynamic model with the bilinear nature for the boost converters [3]. Under the assumption of ideal *infinite* switching frequency operation, the combined model can be interpreted as an *average model* with a continuous and bounded control input [2], [3]. This model makes possible the nonlinear control methods to be applied. Generally, these control methods can be decomposed into *direct* and *indirect* control design for the dc–dc boost converter [2]. The direct methods mainly rely on feedback from the output voltage and are sensitive to the input voltage measurements. In contrast, the indirect methods require feedback from the input current and are sensitive to the load variations. It is shown in [3, Secs. 3.3 and 5.2] that the *sliding mode* and the *input–output feedback linearization* control methodologies based on direct method do not work due to imposing the unstable zero dynamics. Hence, the indirect method is used to stabilize the output of the system [3]. *Passivity-based* (PB) control methods are one of the widely used methods for stabilizing the system. Another indirect control design is the dynamic PB controller proposed in [3, Sec. 5.3] that uses the energy shaping plus damping injection technique to derive the control law. A static PB controller corresponding to Hamiltonian stabilization error representation is designed in [3, Sec. 5.4]. A saturated type of the static controller is presented in [2, Sec. 8.3]. In [7], an observer-based controller is designed to improve the control performance by estimating and canceling the disturbance owing to the plant-model mismatch. The instrumental assumption in the construction of the observer is that the disturbance converges to a constant value. Also, digital hybrid and optimal control techniques are used for the benchmark problem [8]–[10]. Five hybrid and optimal control techniques, including predictive control, robust control, relaxed dynamic programing, and Lyapunov function-based stabilizing control, are experimentally compared with the dc–dc boost converter in [8]. The controllers show similar dynamic performance, and most differences are related to the tuning of the controller. The model predictive controller proposed in [9] minimizes a cost function without the need for a numerical algorithm in its corresponding online solution. However, the performance of such a model predictive controller practically can be limited by the memory allocation, which is needed for the prediction horizon. Moreover, most of these methods are sensitive to the parametric mismatch which can act as a disturbance. It is worth pointing out that the feedback linearization controller in [3], the static PB controller in [2] and [3], the disturbance observer-based controller in [7], and the digital controllers in [8]–[10] require the measurements of both states, the input current and the output voltage. In contrast, the sliding mode

Manuscript received October 13, 2020; accepted December 7, 2020. Manuscript received in final form December 10, 2020. Recommended by Associate Editor G. Pin. *(Corresponding author: Mehdi Tavan.)*

Mehdi Tavan is with the Department of Electrical Engineering, Nour Branch, Islamic Azad University, Nour 4641859557, Iran (e-mail: m.tavan@srbiau.ac.ir).

Kamel Sabahi is with the Department of Engineering Sciences, Faculty of Advanced Technologies, University of Mohaghegh Ardabili, Namin 5619911367, Iran (e-mail: k.sabahi@uma.ac.ir).

Amin Hajizadeh, Mohsen N. Soltani, and Kasper Jessen are with the Department of Energy Technology, Aalborg University, 6700 Esbjerg, Denmark (e-mail: aha@et.aau.dk; sms@et.aau.dk; kje@et.aau.dk).

Color versions of one or more figures in this article are available at https://doi.org/10.1109/TCST.2020.3044378.

Digital Object Identifier 10.1109/TCST.2020.3044378

controller and the dynamic PB controller in [3] only need the input current measurement. Recently, an embedded pulsewidth modulation (PWM) approach is introduced in [11]. The convergence of the control approach in both model-based and adaptive versions is examined using the linear matrix inequality (LMI) conditions. The method is applied to a flyback dc–dc converter to control the system under parametric uncertainty in the input and output sides. A *Luenberger*-type observer is employed to estimate the unknown parameters by the injection error between the states and their estimates. Also, it can be shown that the proposed LMI-based observer is able to estimate the input current and the input voltage simultaneously.

Due to the dc property of the input current, usually, Hall effect current sensors have been used to measure the input current [9]. It is well known that the current sensors' performance is sensitive to the stray magnetic fields, large temperature drift, and large offset voltage. In contrast, from a practical viewpoint, it is simple and convenient to measure the output voltage. Hence, current observer-based controllers are designed to make the control procedure reliable and cost-effective by eliminating the current sensor. Luenberger-type observer is introduced in [3, Sec. 5.7] to estimate the input current. The estimation error dynamics for the proposed observer forms a lower triangular system with only one gain for pole placement. A drawback of the proposed observer is that the convergence rate is limited, and then the transient response cannot be improved arbitrarily. This weakness can also be observed in the unified robust observer introduced in [12]. A reduced-order observer is presented in [3, Sec. 5.8]. The observer can be interpreted as an *immersion and invariance* (I&I)-based observer, and its convergence rate can be increased arbitrarily. An estimation of the input current is obtained by the *integral reconstructor* method in [3, Sec. 5.9]. The estimator only needs the measurements of the input and output voltages. Unfortunately, the technique uses an *open-loop* integration, which thwarts the practical applications of this method in the presence of measurement noise. For instance, unbounded signals can be generated when the measurements are corrupted by a constant bias (see Remark R5 in [13] and the simulation results in [14]).

For a specified desired output voltage, the transmission of energy from input to the output implies that the desired input current is directly related to the output load conductance and inversely to the input voltage. In many applications, the output load is unknown or time-varying, in which case an extra output current sensor is required to measure it. Hence, adding adaptation to the preceding current observers to estimate the output load conductance making their practical implementation more attractive. The obstacle in developing such an adaptive observer is that uncertainty appears in the output dynamics in the boost converter.

In the classical procedures to the design of an adaptive observer, the parametric uncertainty in the output dynamics can impose a manifold of equilibria in some cases. In this manner, the convergence of the state and parameter estimation depends upon fulfilling an *excitation* condition, which is hard to verify in real applications. Hence, the control design procedure is hampered by an obstacle known as *detectability*. This difficulty is at the core of the convergence problem of the system in closed-loop with the adaptive observer and a full-information controller (see [15] and [2, Sec. 3.3] for more detail). For example, the classical adaptive observer introduced for ac–dc boost converter in [16] lies in this situation, so the obtained results lack scientific support. However, in this case, the *persistent excitation* (PE) condition can be satisfied if the controlled system reaches its desired responses. Unfortunately, for the regulation problem of the dc–dc boost converter, the desired response does not satisfy even the PE condition, and this makes the problem more challenging. Hence, some output feedback control algorithms are proposed to circumvent these obstacles, such as [2], [3], and [17]–[22].

The I&I technique is employed in [2] and [17] to estimate the input current and voltage for the dc–dc boost converter. Although the I&I adaptive observer needs *a priori* knowledge about the output load conductance, the closed-loop system locally achieves the output voltage regulation despite the load uncertainty with a certain range. The integral reconstructor estimator is used in conjunction with a sliding mode controller in [3], which needs the value of the output load conductance to extract the desired input current. The overall closed-loop control system is locally asymptotically stable, and the experimental results in [3] show a robust performance against variations in the output load. The *passivity-based* (PB) control design methodology has been widely applied to the dc–dc boost converter [18]–[20]. A simple static nonlinear output feedback controller based on interconnection and damping assignment PB control methodology has been introduced in [19]. Although the PB controller is insensitive to the load varying, it is sensitive to variations in the input voltage. The lack of integral action in the proposed controller makes it inadequate for the practical applications from the conventional wisdom. Hence, an adaptation law is added to the controller in [19] and [23], which needs the measurements of the input current. The parallel-damped PB control method is employed in [18] to form a dynamic output feedback controller, which needs *a priori* knowledge about the load conductance. The controller designed in [18] was developed to a simplified linearized version in [20]. In this method, the controller parameters were required to be adjusted when the output load deviates from the nominal value. A complementary PID controller to the proposed controller [20] is designed in [21] to compensate for the disturbance owing to the parasitic resistance. Both the controller in [20] and [21] are locally convergent, and *a priori* knowledge about the load conductance is required. In [22], it is shown that the *proportional-integral* (PI) output feedback controller semiglobally achieves the control objectives for sufficiently small proportional gain. However, the integral gain is restricted to an upper bound, which depends on the initial conditions and the system parameters.

This brief addresses a solution to the problem of the output feedback control of dc–dc boost converter with unknown load conductance. First, a full-information dynamic controller, with uniformly globally asymptotically stability (UGAS), is proposed. Subsequently, an adaptive observer is designed to render the scheme adaptive. Instrumental for the construction of the observer relies on the introduction of a new I&I-based

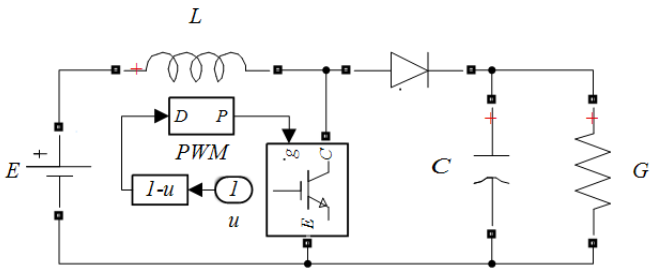

Fig. 1. DC–dc boost converter circuit.

filtered transformation, which immerses the system dynamics to a proper adaptive form. Although the transformation poses an overparameterization, the detectability obstacle in the closed-loop stability analysis is overcome without any restrictive assumption on the system behavior. The main contributions of the present brief are listed as follows.

1) The proposed I&I observer guarantees the parametric convergence under the nonsquare integrability condition, which is weaker than the usual PE one.
2) To implement the proposed control scheme, just two voltage sensors and the values of the inductance/capacitance are required.
3) The proposed control algorithm is experimentally validated on a prototype dc–dc boost converter under changes in the load, input source, and desired output.

The remaining of this brief is structured in the following way. In Section II, the model of system and the problem statement are presented. Section III introduced the proposed control algorithm and its stability analysis. In Section IV, besides the experimental results, realistic simulations are added to compare the performance of the controller with the one in [19] and [22]. Finally, this brief is closed by the conclusions of Section V.

II. Dynamic Model and Problem Statement

Consider the electric circuit of the dc–dc boost depicted in Fig. 1. The semiconductors are considered ideal, and the switching signal P is generated by a PWM circuit, which takes values in finite set $\{0, 1\}$. Using Kirchhoff's laws, the average model of the dc–dc boost converter can be described by the following bilinear type system [3]:

$$L\dot{i} = E - u\upsilon \tag{1}$$

$$C\dot{\upsilon} = ui - G\upsilon \tag{2}$$

where $\upsilon(t)$ is the output (capacitor) voltage; $i(t)$ is the input (inductor) current; C, L, G, and E are positive constants representing the capacitance, inductance, load conductance, and input voltage, respectively. Finally, $u(t) \in [\epsilon, 1]$, with $0 < \epsilon < 1$, is the continuous control signal, which represents the duty ratio of the transistor switch.

Assumption 1: We assume that the parameters C and L are known. Also, just two voltage sensors are available to measure the output voltage υ and the input voltage E.

For the system (1) and (2) under Assumption 1, the control objective is to regulate the output voltage on a desired constant value $V_d \geq E$. An adaptive controller is expected to achieve the objective, since the adaptation can compensate for the modeling mismatch, such as the parasitic resistances.

III. Proposed Control Algorithm

Our control algorithm is formed by connecting the converter system in a closed-loop with a full-information dynamic controller in conjunction with an adaptive observer. This creates an adaptive dynamic output feedback controller, which satisfies the control objective. To improve readability, this section is decomposed into three sections. Section III-A presents our full-information saturated controller and its stability analysis. The adaptive I&I-based observer is introduced in Section III-B. Finally, in Section III-C, the control algorithm is constituted by combining the full-information controller and the adaptive observer, and the closed-loop stability analysis completes this part.

A. Full-Information Saturated Controller

By setting υ to the desired constant value in (1) and (2), the equilibrium operating point can be obtained as [3]

$$\upsilon = V_d \Rightarrow i_d = GV_d^2E^{-1}, \quad u_d = V_d^{-1}E. \tag{3}$$

The following proposition proposes a full-information saturated controller that regulates the system at the equilibrium operating point.

Proposition 1: Consider the dc–dc boost converter described by (1) and (2) in closed-loop with the dynamic control law

$$u = \sigma(w) \tag{4}$$

$$\dot{w} = -\lambda_1 w + Ei - GV_d\upsilon \tag{5}$$

where the saturation function $\sigma : \mathbb{R} \to [\epsilon, 1]$ is differentiable and satisfies

$$\sigma(0) = u_d \tag{6}$$

$$w(\sigma(w) - u_d) > 0 \tag{7}$$

for all nonzero value of w and $u_d \in [\epsilon, 1]$, and the additional condition

$$\int_0^w (\sigma(\tau) - u_d)\mathrm{d}\tau \to \infty \text{ as } |w| \to \infty. \tag{8}$$

Then, for any $\lambda_1 \in \mathbb{R}_{>0}$ and $w(0) \in \mathbb{R}$, the equilibrium (V_d, i_d) is uniformly globally asymptotically stable.

Proof 1: To facilitate the stability analysis, we define the function

$$\begin{aligned}\psi(w) &= \sigma(w) - u_d \\ &= u - u_d.\end{aligned} \tag{9}$$

It is clear that $|\psi(w)| < 1$ and $\psi(0) = 0$. Now, consider the proper Lyapunov function

$$\mathcal{H}_c(\tilde{\upsilon}, \tilde{i}, w) = \frac{1}{2}C\tilde{\upsilon}^2 + \frac{1}{2}L\tilde{i}^2 + \frac{V_d}{E}\int_0^w \psi(\tau)\mathrm{d}\tau \tag{10}$$

where $\tilde{\upsilon} = V_d - \upsilon$ and $\tilde{i} = i_d - i$. Note that the last term in the above equation is always positive for nonzero w and *radially unbounded* due to (7) and (8), respectively. The time

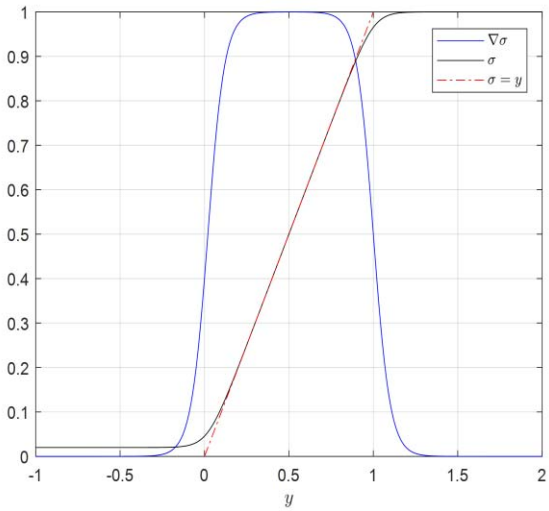

Fig. 2. Proposed saturation function and its derivative for $a = 10$ and $\epsilon = 0.02$.

derivative of (10) along the trajectories of (1), (2), and (5) is given by

$$\begin{aligned}\dot{\mathcal{H}}_c &= -G\tilde{v}^2 - \frac{V_d}{E}\psi(w)(Ei - GV_d v) + \frac{V_d}{E}\psi(w)\dot{w} \\ &= -G\tilde{v}^2 - \frac{V_d}{E}\lambda_1 w\psi(w) \le 0 \end{aligned} \tag{11}$$

which implies that $\tilde{v}, \tilde{i}$, and w are bounded. Notice that the system (1) and (2) in closed-loop with (4) and (5) is autonomous, so by applying *LaSalle's theorem* [24], we can conclude that $\tilde{v}$ and w asymptotically converge to zero, and in its turn, from (3), i converges to i_d. Because the closed-loop system is autonomous and $\mathcal{H}_c$ is radially unbounded, the convergence properties are uniform and global, respectively. This completes the proof.

Remark 1: An example of the saturation function σ, which satisfies the conditions (6)–(8), is the one introduced in Proposition 8.6 in [2]. We present the following smooth function:

$$\sigma(y) = \frac{1}{2}\left(1 + \epsilon + \frac{1}{a}\ln\frac{\cosh a(y-\epsilon)}{\cosh a(y-1+\epsilon)}\right) \tag{12}$$

where $a \in \mathbb{R}_{>0}$ is sufficiently large to verify (6). The derivative of the function is given by

$$\nabla\sigma = \frac{1}{2}(\tanh a(y-\epsilon) - \tanh a(y-1+\epsilon)). \tag{13}$$

Fig. 2 shows the behavior of the function and its derivative for $a = 10$ and $\epsilon = 0.02$.

B. I&I Adaptive Observer

The objective of this section is to construct an adaptive observer that ensures, under suitable assumptions, converging estimates for the unmeasured state i and the unknown parameter G. To provide a proper adaptive form, the following input–output filtered transformation is considered:

$$\boldsymbol{\iota} := i - G\boldsymbol{\upsilon} \tag{14}$$

where $\boldsymbol{\upsilon} : \mathbb{R}_+ \to \mathbb{R}$ is an auxiliary dynamic vector, which its dynamics are to be defined. The equation above admits the global inverse

$$\begin{aligned} i &= \boldsymbol{\iota} + G\boldsymbol{\upsilon} \\ &= \begin{bmatrix} 1 & \boldsymbol{\upsilon} \end{bmatrix}\eta \end{aligned} \tag{15}$$

where

$$\eta := \mathrm{col}(\boldsymbol{\iota}, G) \tag{16}$$

is the new unavailable vector. The dc–dc boost converter system (1) and (2) can be rewritten in terms of the new variables as

$$\dot{\eta} = \begin{bmatrix} 0 & -\dot{\boldsymbol{\upsilon}} \\ 0 & 0 \end{bmatrix}\eta + \frac{1}{L}\begin{bmatrix} E - u v \\ 0 \end{bmatrix} \tag{17}$$

$$\dot{v} = \frac{1}{C}[u \quad u\boldsymbol{\upsilon} - v]\eta. \tag{18}$$

Proposition 2: Consider the dc–dc boost converter model (17) and (18) and the observer

$$\begin{aligned} \dot{\zeta}_1 &= -u\begin{bmatrix}\kappa_1 & -\kappa_3(u\boldsymbol{\upsilon} - v)\end{bmatrix}(\zeta + \beta) + L^{-1}(E - uv) \\ \dot{\zeta}_2 &= -\kappa_2\big((u\boldsymbol{\upsilon} - v)\begin{bmatrix} u & u\boldsymbol{\upsilon} - v\end{bmatrix}(\zeta + \beta) + Cv(\boldsymbol{\upsilon}\dot{u} + \dot{\boldsymbol{\upsilon}}u)\big) \end{aligned} \tag{19}$$

$$\dot{\boldsymbol{\upsilon}} = -(\kappa_1 + \kappa_3 u)(u\boldsymbol{\upsilon} - v) \tag{20}$$

with $\zeta = [\zeta_1 \quad \zeta_2]^{\mathrm{T}}$ as the observer states and the mapping

$$\beta(v, t) = \begin{bmatrix} Cv\kappa_1 \\ C\big(vu\boldsymbol{\upsilon} - 0.5v^2\big)\kappa_2 \end{bmatrix}. \tag{21}$$

Let

$$\hat{\boldsymbol{\iota}} = \zeta_1 + Cv\kappa_1 \tag{22}$$

$$\hat{G} = \zeta_2 + C\big(vu\boldsymbol{\upsilon} - 0.5\, v^2\big)\kappa_2 \tag{23}$$

$$\hat{i} = \begin{bmatrix} 1 & \boldsymbol{\upsilon}\end{bmatrix}(\zeta + \beta) \tag{24}$$

be the estimate of $\boldsymbol{\iota}$, G, and i, respectively. Then, for any positive constants, κ_1, κ_2, and κ_3, $\bar{G} = G - \hat{G}$, and $\bar{\boldsymbol{\iota}} = \boldsymbol{\iota} - \hat{\boldsymbol{\iota}}$ are globally bounded. Also, if v is bounded, then $\bar{\boldsymbol{\iota}}$ asymptotically converges to zero. Moreover, if $u\boldsymbol{\upsilon} - v$ is not square-integrable, then $\bar{G}$ and $\bar{i} = i - \hat{i}$ asymptotically converge to zero.

Proof 2: To begin with, under the inspiration of the I&I technique [2], let us define the estimation errors as

$$\bar{\eta} = \eta - \zeta - \beta(v, t) \tag{25}$$

where $\bar{\eta} = [\bar{\boldsymbol{\iota}} \quad \bar{G}]$ concerning (22) and (23). Differentiating (25) and using (17)–(21) yields to

$$\dot{\bar{\eta}} = -\begin{bmatrix} \kappa_1 u & -\kappa_3 u(u\boldsymbol{\upsilon} - v) \\ \kappa_2 u(u\boldsymbol{\upsilon} - v) & \kappa_2(u\boldsymbol{\upsilon} - v)^2 \end{bmatrix}\bar{\eta} \tag{26}$$

which has the form of a damped nonlinear oscillator. Evaluating the time derivate of the Lyapunov function

$$\begin{aligned} \mathcal{H}_o(\bar{\boldsymbol{\iota}}, \bar{G}) &= \frac{1}{2}\bar{\boldsymbol{\iota}}^2 + \frac{1}{2}\frac{\kappa_3}{\kappa_2}\bar{G}^2 \\ &= \frac{1}{2}\bar{\eta}^T \mathrm{diag}\big(1, \kappa_3\kappa_2^{-1}\big)\bar{\eta} \end{aligned} \tag{27}$$

along the trajectories of (26) satisfies

$$\begin{aligned} \dot{\mathcal{H}}_o &= -\kappa_1 u\bar{\boldsymbol{\iota}}^2 - \kappa_3(u\boldsymbol{\upsilon} - v)^2\bar{G}^2 \\ &= -\bar{\eta}^T \mathrm{diag}\big(\kappa_1 u, \kappa_3(u\boldsymbol{\upsilon} - v)^2\big)\bar{\eta} \le 0 \end{aligned} \tag{28}$$

which implies that $\bar{\imath}$ and $\bar{G}$ are bounded. Notice that the error dynamic (26) is a nonautonomous system because of its dependence on the time-varying signals u and υ. Therefore, instead of LaSalle's theorem, the generalization of *Barbalat's lemma* in [25] is invoked here. From (28), it can be concluded that $\bar{\imath}$ and $(u\boldsymbol{\upsilon}-\upsilon)\bar{G}$ are square-integrable.

Now note that by setting $\upsilon = V_d$ and $u = u_d$ in (20), the desired steady-state value of $\boldsymbol{\upsilon}$ can be obtained as

$$\begin{aligned}\boldsymbol{\upsilon}_d &= u_d^{-1}V_d \\ &= E^{-1}V_d^2. \end{aligned} \tag{29}$$

Consider the proper Lyapunov function

$$\mathcal{H}_a(\tilde{\upsilon}) = \frac{1}{2}\tilde{\upsilon}^2 \tag{30}$$

where $\tilde{\boldsymbol{\upsilon}} = \boldsymbol{\upsilon}_d - \boldsymbol{\upsilon}$. Using (20), the time derivative of (29) is such that

$$\begin{aligned}\dot{\mathcal{H}}_a &= \tilde{\upsilon}(\kappa_1+\kappa_3 u)(u\boldsymbol{\upsilon}-\upsilon) \\ &= -(\kappa_1+\kappa_3 u)\big(u\tilde{\upsilon}^2 - \tilde{\upsilon}\boldsymbol{\upsilon}_d\psi(w) + \tilde{\upsilon}\tilde{\upsilon}\big) \\ &\le -(\kappa_1+\kappa_3 u)\left(\frac{u}{2}\tilde{\upsilon}^2 - \frac{1}{u}(\boldsymbol{\upsilon}_d\psi)^2 - \frac{1}{u}\tilde{\upsilon}^2\right) \end{aligned} \tag{31}$$

where Young's inequality has been applied to get the last inequality. From (31), we can conclude that if υ is bounded, then $\boldsymbol{\upsilon}$ remains bounded.Consequently, the term $u\boldsymbol{\upsilon}-\upsilon$ is bounded.

Using the above result in (26), it can be obtained that $\dot{\tilde{\eta}}$ is bounded. As a result, $\dot{\tilde{\imath}}$ is bounded and regarding the square integrability and boundedness of $\bar{\imath}$, its uniform convergence to zero can be concluded from [25]. Finally, if $u\boldsymbol{\upsilon}-\upsilon$ is not square-integrable, the time derivative of $\mathcal{H}_o$ in (28) satisfies

$$\dot{\mathcal{H}}_o \le -\varrho(t)^2\mathcal{H}_o \tag{32}$$

for some nonsquare integrable function $\varrho(t)$. Solving this simple scalar differential equation, we get $\mathcal{H}_o$ converges to zero, which implies $\bar{\imath}$ and $\bar{G}$ converge to zero. The proof is completed by noting that $\tilde{\imath} = \bar{\imath} + \boldsymbol{\upsilon}\bar{G}$.

Remark 2: In the proposed adaptive observer, the parametric convergence, instead of the usual PE condition, requires that the signal $u\boldsymbol{\upsilon}-\upsilon$ is not square-integrable. It is well known that the new requirement is less restrictive (see [26] and [27] for some examples).

C. Stability Analysis of the Closed-Loop System

The certainly equivalent of the full-information controller (4) and (5) of Proposition 1 is formed substituting i and G by their estimates $\hat{\imath}$ and $\hat{G}$, derived from the adaptive observer of Proposition 2, as

$$\dot{w} = -\lambda_1 w + E\hat{\imath} - \hat{G}V_d\upsilon. \tag{33}$$

Note that the ζ_2-dynamics in (19) requires the u-dynamics, which regarding (4) and (33) is given by

$$\begin{aligned}\dot{u} &= \nabla\sigma\,\dot{w} \\ &= \nabla\sigma\big(-\lambda_1 w + E\hat{\imath} - \hat{G}V_d\upsilon\big). \end{aligned} \tag{34}$$

Fig. 3 demonstrates the implementation of the proposed control algorithm.

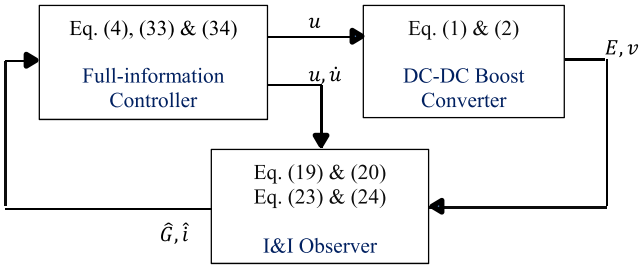

Fig. 3. Closed-loop system implementation of the proposed algorithm.

Proposition 3: Consider the dc–dc boost converter (1) and (2) in closed-loop with (4), (19), (20), (23), (24), and (33). Then, there exists a $\lambda_s > 0$ such that for any positive constants κ_1, κ_2, κ_3, and $\lambda_1 \ge \lambda_s$, all signal are bounded and the equilibrium point $(\tilde{\upsilon}, \tilde{\imath}) = 0$ is UGAS.

Proof 3: To begin with, note that (33) can be rewritten as

$$\begin{aligned}\dot{w} = -\lambda_1 w + Ei - GV_d\upsilon + E\bar{\imath} - V_d(u\boldsymbol{\upsilon}-\upsilon)\bar{G} \\ + V_d(\boldsymbol{\upsilon}_d - \tilde{\upsilon})\psi(w)\bar{G} \end{aligned} \tag{35}$$

which is the sum of (5) and the terms of mismatch perturbations. It is worth pointing out that $\bar{\imath}$ and $\bar{G}$ are bounded from Proposition 2. Now, consider the proper Lyapunov function

$$\mathcal{H}(\tilde{\upsilon},\tilde{\imath},w,\bar{\imath},\bar{G},\tilde{\upsilon}) = \mathcal{H}_c(\tilde{\upsilon},\tilde{\imath},w) + \mathcal{H}_o(\bar{\imath},\bar{G}) + \frac{1}{2}\frac{G}{\kappa_3}\mathcal{H}_a(\tilde{\upsilon}) \tag{36}$$

where the functions $\mathcal{H}_c$, $\mathcal{H}_o$, and $\mathcal{H}_a$ have been defined in (10), (27), and (30), respectively. The time derivatives of $\mathcal{H}$ can be obtained by substituting (35) in (11) and adding its result to the sum of (28) and (31) as

$$\begin{aligned}\dot{\mathcal{H}} \le -G\tilde{\upsilon}^2 - \frac{V_d}{E}\lambda_1 w\psi(w) - \kappa_1 u\bar{\imath}^2 - \kappa_3(u\boldsymbol{\upsilon}-\upsilon)^2\bar{G}^2 \\ - \frac{1}{2}G\left(\frac{u^2}{2}\tilde{\upsilon}^2 - (\boldsymbol{\upsilon}_d\psi)^2 - \tilde{\upsilon}^2\right) \\ + \psi\big(V_d\bar{\imath} - \boldsymbol{\upsilon}_d(u\boldsymbol{\upsilon}-\upsilon)\bar{G}\big) + \boldsymbol{\upsilon}_d(\boldsymbol{\upsilon}_d-\tilde{\upsilon})\psi^2\bar{G} \end{aligned} \tag{37}$$

where some basic bounding has been done. Now, applying Young's inequality in (37) yields to

$$\begin{aligned}\dot{\mathcal{H}} \le -\frac{G}{2}\tilde{\upsilon}^2 - \frac{\kappa_1}{2}u\bar{\imath}^2 - \frac{\kappa_3}{2}(u\boldsymbol{\upsilon}-\upsilon)^2\bar{G}^2 - \frac{G}{8}u^2\tilde{\upsilon}^2 \\ - \psi(w)\left(\frac{V_d}{E}\lambda_1 w - \frac{1}{2}d\psi(w)\right) \end{aligned} \tag{38}$$

with

$$d = \frac{V_d^2}{\kappa_1 u} + \left(\frac{1}{\kappa_3} + G + 2\bar{G} + \frac{4}{G}\left(\frac{\bar{G}}{u}\right)^2\right)\boldsymbol{\upsilon}_d^2. \tag{39}$$

Not that d is bounded because $\bar{G}$ is bounded and $u \in [\epsilon, 1]$. So, boundedness of $\tilde{\upsilon}$, $\tilde{\imath}$, w, and $\tilde{\upsilon}$ can be concluded from (38) regarding (7) and $|\psi(w)| < 1$. Finally, differentiability of ψ implies that there exist some positve constants λ_s and λ_h such that for any $\lambda_1 \ge \lambda_s$, (38) satisfies

$$\begin{aligned}\dot{\mathcal{H}} \le -\frac{\kappa_1}{2}u\bar{\imath}^2 - \frac{\kappa_3}{2}(u\boldsymbol{\upsilon}-\upsilon)^2\bar{G}^2 - \frac{G}{8}u^2\tilde{\upsilon}^2 \\ - \frac{G}{2}\tilde{\upsilon}^2 - \lambda_h w\psi(w) \le 0. \end{aligned} \tag{40}$$

TABLE I
PARAMETERS VALUES OF THE SYSTEM USED IN THE SIMULATION AND EXPERIMENT

Parameters	Value	Unit
E	60	V
L	478	μH
C	130	μF
G	1/110	S
V_d	90	V

By noting that the closed-loop system is autonomous, applying LaSalle's theorem to (40), we can conclude that $\bar{\imath}$, $(u\boldsymbol{\upsilon}-\upsilon)\bar{G}$, $\tilde{\upsilon}$, $\tilde{\upsilon}$, w, and in its turn $\tilde{i}$ asymptotically converges to zero. Since the closed-loop system is autonomous, and $\hat{h}$ is radially unbounded, these properties are uniform and global. This establishes the claim.

Remark 3: Notice that $\tilde{\upsilon} = 0$ implies, from (20), that $u\boldsymbol{\upsilon} = \upsilon$. Consequently, the convergence of $\bar{G}$ to zero is not guaranteed from Proposition 2. However, the perturbations caused by the parameter mismatch converge to zero in (35), since the closed-loop system ensures that $u\boldsymbol{\upsilon} - \upsilon$ and w uniformly asymptotically converge to zero.

Remark 4: The term $Ei - GV_d\upsilon$ in (5) can be interpreted as the difference between the input and output power. From (15), the auxiliary variable $\boldsymbol{\upsilon}$ is in volt, and from (20), it can be interpreted as a filtered version of υ. The component w generated by the dynamic (33) can be interpreted as a filter version of the error term $E\hat{i} - \hat{G}V_d\upsilon$. So, a proper value of λ_1 can prevent aliasing the feedback signals by high-frequency additive perturbations.

Remark 5: It is worth pointing out that the Lyapunov argument confirming uniform asymptotic stability of the control system implies, by the way of total stability arguments, robustness with respect to the bounded disturbances, and the additive perturbations on the measured signals E and υ. In the presence of uncertainty in the inductance and capacitance values, the estimation errors do not converge to zero. Note that although the uncertainty can be incorporated in κ_1 and κ_2 in (21)–(24), it imposes a bounded disturbance in the observer dynamics due to the last terms in (19), which are multiplied by L^{-1} and C. Hence, the estimated variables in the control law (33) are perturbed. However, the system trajectories remain bounded due to the *uniform* version of stability of the closed-loop system.

IV. SIMULATION AND EXPERIMENTAL RESULTS

Simulations are performed using MATLAB-Simulink Simscape Power System–with the parameters of a real dc–dc boost converter listed in Table I. The I&I-based adaptive output feedback controller used in this section is given by

$$u = \sigma(u_d + \lambda_2 w) \tag{41}$$

where λ_2 is a positive constant, $\sigma(.)$ is defined in (12), and w is generated by (33). The performance of the proposed controller is compared with two output feedback control algorithms introduced in [19] and [22]. The controllers satisfy the asymptotic regulation of the output voltage by only feedback from the output voltage and they are insensitive to uncertainty in the load resistance, like the one introduced in this brief. The control laws of the PI controller in [22] and the PB controller in [19] are, respectively, given by

$$u = u_d + k_P\tilde{\upsilon} + k_I\int_0^t \tilde{\upsilon}(\tau)\mathrm{d}\tau \tag{42}$$

$$u = u_d\left(\frac{\upsilon}{V_d}\right)^{\alpha} \tag{43}$$

where k_P and k_I are positive constants, and $0 < \alpha < 1$, although the closed-loop system remains stable for $-1 < \alpha < 0$. Finally, experimental results are concluded on a prototype dc–dc boost converter to support the simulation results.

A. Simulation Results

The simulations' objective is to evaluate the performance of the above control algorithms against changes in desired voltage, output load, and input voltage. The switching frequency of the PWM is set to 40 kHz. All initial values are set to zero.

The best performance of the PB controller is accomplished by $\alpha = -0.117$. Notice that the convergence speed decreases for a positive value of α. The PI controller gains are obtained by trial and error as $k_P = 1\times10^{-3}$ and $k_I = 1\times10^{-10}$. As notified in [22], the proportional gain k_P must be small enough to ensure asymptotic regulation. The I&I controller gains are set to $\lambda_1 = 20\times10^3$, $\lambda_2 = 7$, $\kappa_1 = \lambda_1$, $\kappa_2 = 10^{-2}$, and $\kappa_3 = 1$. It is worth pointing out that κ_is are tuned such that to generate a fast estimation. Also, according to Proposition 3, a large value of λ_1 is desired to make the error dynamics stable. On the other hand, regarding Remark 4, λ_1 is suggested to be smaller than the PWM frequency to attenuate the chattering of the measured signals. Finally, whereas a small value of λ_2 reduces the effect of feedback, a very large value deteriorates the performance due to the saturation of the control input. Hence, a balance between the saturation bounds and the desired duty cycle is needed to tune λ_2.

Figs. 4 and 5 show the performance of the controllers in the phase of change to $V_d = 120$ V at $t = 0.05$ s, change to $G = 1/55$ S at $t = 0.1$ s, and change to $E = 80$ V at $t = 0.15$ s. Figs. 4 and 5 depict the time histories of the output voltage and the input current, respectively. Although the PB and PI controllers have a simple structure, the proposed I&I controller demonstrates significantly better performance by comparison. Both the PI and PB controllers pose a big overshot and oscillations in response to the changes. This is because both of the controllers follow a *direct* strategy in the output regulation, while the system is the nonminimum-phase with respect to the output. In comparison, the proposed I&I controller pursues an *indirect* strategy that uses an estimation of the input current in the control law. Hence, the transient response in Fig. 4 demonstrates a fast convergence for the I&I controller after the changes.

Fig. 6 shows the time history of $\bar{\imath}$, $\bar{G}$, $u\boldsymbol{\upsilon} - \upsilon$, and w associated with the proposed I&I controller. The simulation

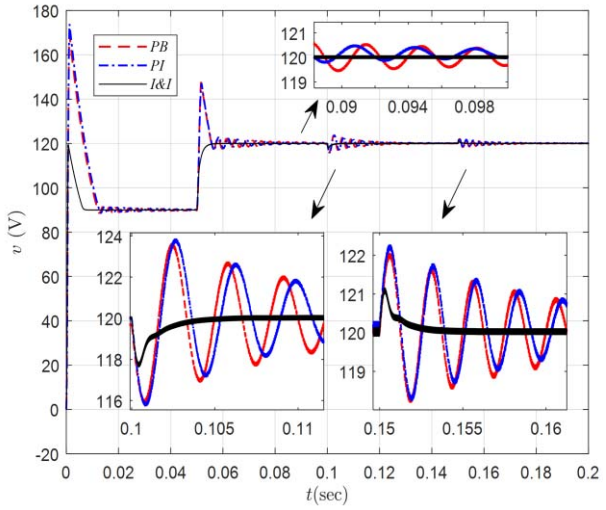

Fig. 4. Time history of the output voltage for changes in V_d, G, and E.

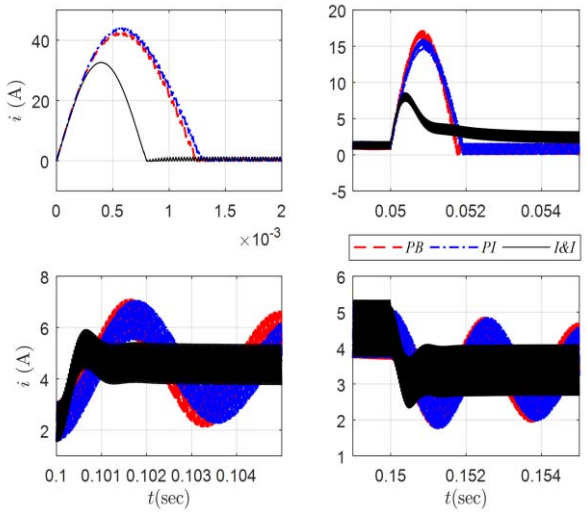

Fig. 5. Time history of the input current for changes in V_d, G, and E.

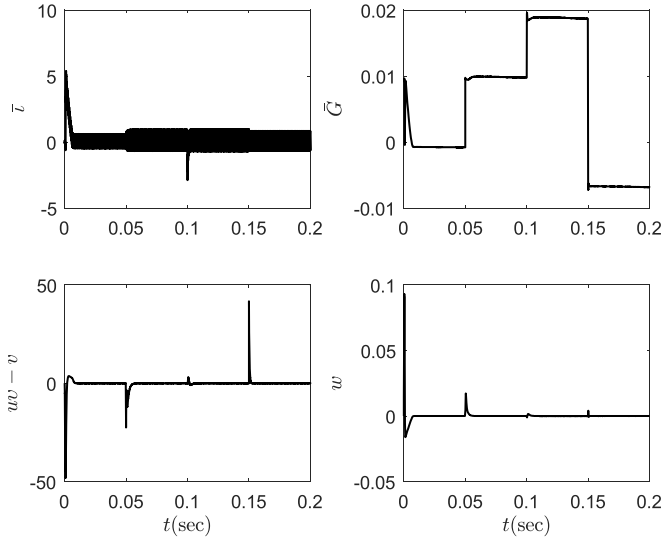

Fig. 6. Time history of $\bar{\imath}$, $\bar{G}$, $uv - v$, and w for changes in V_d, G, and E.

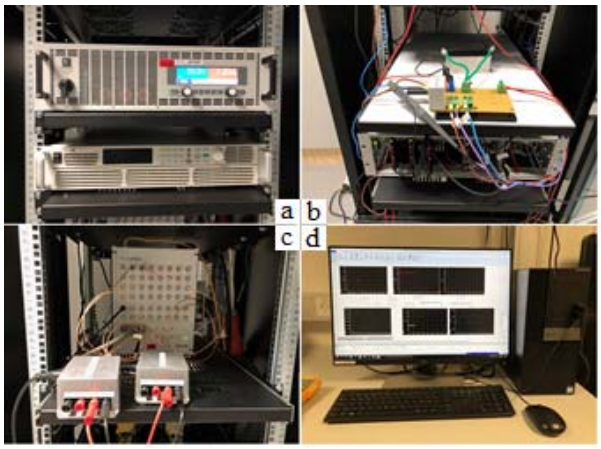

Fig. 7. Experimental equipment. (a) DC power. (b) DC–dc boost converter. (c) dSPACE setup and sensors. (d) Computer.

shows that the estimation error $\bar{\imath}$ converges to zero very fast. Its time history shows a chattering of frequency 40 kHz around zero that is related to the PWM switching effect on the inductor current. The time history of $\bar{G}$ shows a steady-state error in Fig. 6. However, as mentioned in Remark 3, the performance of the closed-loop system is not affected by the error, since $u\boldsymbol{v}-v$ and w converge to zero, as demonstrated in Fig. 6.

B. Experimental Results

To examine the performance of the proposed I&I-based adaptive output feedback controller, the experimental tests are carried out, with the same scenario as simulated above, on the setup shown in Fig. 7. The converter that is employed for experiments is PEB 4046 Imperix product. The designed interface and protection card (IPC) of the converter from Aalborg University is used to implement the real-time control. This IPC is digitally driven by a dSPACE DS1104 board, where the control algorithm is implemented using the C-code generated by the Real-time Workshop Target Simulink Library. The switching frequency of the PWM is set to 40 kHz. The converter and the controller parameters and initial conditions are the same as those used in simulations.

The results of the experimental tests are shown in Figs. 8–10. At the first test, the desired output changes from $V_d = 120$ V to $V_d = 90$ V. As shown in Fig. 8, the closed-loop system tracks the new desired value fast but with a small overshot in comparison with the simulation result. The figure shows that the waveform of the input voltage is aliased by the voltage drop induced by the product of the input current and the parasitic resistance of the voltage source.

The second test evaluates the performance of the controller against the load variation from $G = 1/110$ S to $G = 1/55$ S. The waveform of the output voltage, shown in Fig. 9, illustrates a fast and robust response of the control system to the change. Comparison with the simulation results, a small tracking error, less than 1% of the desired output, can be seen in the controller behavior. To interpret this behavior, it is

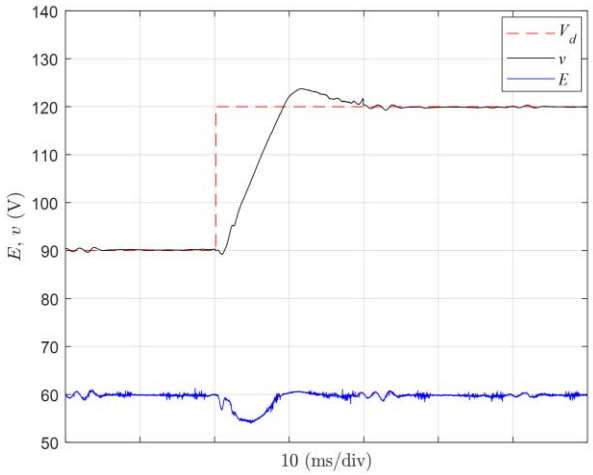

Fig. 8. Experimental waveform of the output and input voltage for a step in V_d from 120 to 90 V.

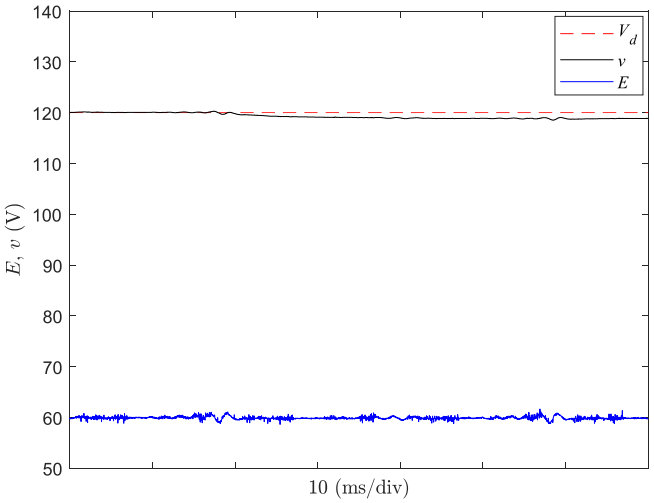

Fig. 9. Experimental waveform of the output and input voltage for changes in G from $1/110$ to $1/55$ S.

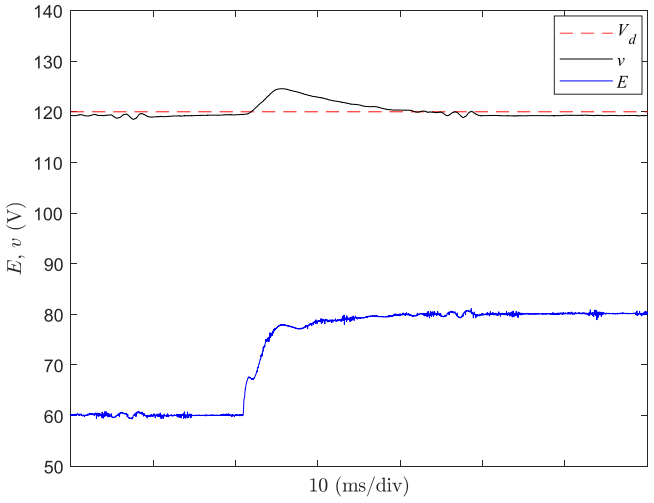

Fig. 10. Experimental waveform of the output and input voltage for a step in E from 80 to 60 V.

important to consider the increase of the input and output current due to increasing the load conductance. This increases the voltage drops by the parasitic resistance in the input and output side, such as transistor and diode resistance, which are not available to consider in the control law.

As shown in Fig. 10, the third test examines the performance of the controller against the input voltage change from $E = 80$ V to $E = 60$ V. The waveform of the output voltage presents a fast transient response of the control system to the change.

V. Conclusion

In this brief, a solution for the detectability obstacle in adaptive output feedback control of the dc–dc boost converter with unknown output load and unavailable input current has been presented. A new insight to circumvent the obstacle has been provided via I&I-based filtered transformation. The proposed transformation yields to an overparameterization, but it immerses the system dynamics to a proper form for adaptive observer design. The designed observer needs the inductance and capacitance values of the system. The control algorithm just requires two voltage sensors, and it achieves significantly better performance in comparison with different control schemes with the same sensors. Current research is underway to generalize this method to a class of bilinear systems, including other commonly used converters topologies.

References

[1] G. Escobar, R. Ortega, H. Sira-Ramírez, J. Vilain, and I. Zein, "An experimental comparison of several nonlinear controllers for power converters," *IEEE Control Syst.*, vol. 19, no. 1, pp. 66–82, Feb. 1999.

[2] A. Astolfi, D. Karagiannis, and R. Ortega, *Nonlinear and Adaptive Control With Applications*. London, U.K.: Springer-Verlag, 2008.

[3] H. Sira-Ramírez and R. Silva-Ortigoza, *Control Design Techniques in Power Electronics Devices*. London, U.K.: Springer-Verlag, 2006.

[4] M. Forouzesh, Y. P. Siwakoti, S. A. Gorji, F. Blaabjerg, and B. Lehman, "Step-up DC–DC converters: A comprehensive review of voltage-boosting techniques, topologies, and applications," *IEEE Trans. Power Electron.*, vol. 32, no. 12, pp. 9143–9178, Dec. 2017.

[5] H. S. Das, C. W. Tan, and A. H. M. Yatim, "Fuel cell hybrid electric vehicles: A review on power conditioning units and topologies," *Renew. Sustain. Energy Rev.*, vol. 76, pp. 268–291, Sep. 2017.

[6] A. Cavallo, G. Canciello, and A. Russo, "Integrated supervised adaptive control for the more electric aircraft," *Automatica*, vol. 117, Jul. 2020, Art. no. 108956.

[7] S.-K. Kim, "Output voltage-tracking controller with performance recovery property for DC/DC boost converters," *IEEE Trans. Control Syst. Technol.*, vol. 27, no. 3, pp. 1301–1307, May 2019.

[8] S. Mariethoz *et al.*, "Comparison of hybrid control techniques for buck and boost DC-DC converters," *IEEE Trans. Control Syst. Technol.*, vol. 18, no. 5, pp. 1126–1145, Sep. 2010.

[9] S.-K. Kim, C. R. Park, J.-S. Kim, and Y. I. Lee, "A stabilizing model predictive controller for voltage regulation of a DC/DC boost converter," *IEEE Trans. Control Syst. Technol.*, vol. 22, no. 5, pp. 2016–2023, Sep. 2014.

[10] J. Saeed and A. Hasan, "Unit prediction horizon binary search-based model predictive control of full-bridge DC–DC converter," *IEEE Trans. Control Syst. Technol.*, vol. 26, no. 2, pp. 463–474, Mar. 2018.

[11] G. Beneux, P. Riedinger, J. Daafouz, and L. Grimaud, "Adaptive stabilization of switched affine systems with unknown equilibrium points: Application to power converters," *Automatica*, vol. 99, pp. 82–91, Jan. 2019.

[12] G. Cimini, G. Ippoliti, G. Orlando, S. Longhi, and R. Miceli, "A unified observer for robust sensorless control of DC–DC converters," *Control Eng. Pract.*, vol. 61, pp. 21–27, Apr. 2017.

[13] R. Ortega, A. Bobtsov, A. Pyrkin, and S. Aranovskiy, "A parameter estimation approach to state observation of nonlinear systems," *Syst. Control Lett.*, vol. 85, pp. 84–94, Nov. 2015.

[14] J. Choi, K. Nam, A. A. Bobtsov, A. Pyrkin, and R. Ortega, "Robust adaptive sensorless control for permanent-magnet synchronous motors," *IEEE Trans. Power Electron.*, vol. 32, no. 5, pp. 3989–3997, May 2017.

[15] E. Panteley, R. Ortega, and P. Moya, "Overcoming the detectability obstacle in certainty equivalence adaptive control," *Automatica*, vol. 38, no. 7, pp. 1125–1132, Jul. 2002.

[16] M. Pahlevani, S. Pan, S. Eren, A. Bakhshai, and P. Jain, "An adaptive nonlinear current observer for boost PFC AC/DC converters," *IEEE Trans. Ind. Electron.*, vol. 61, no. 12, pp. 6720–6729, Dec. 2014.

[17] M. Malekzadeh, A. Khosravi, and M. Tavan, "Immersion and invariance-based filtered transformation with application to estimator design for a class of DC-DC converters," *Trans. Inst. Meas. Control*, vol. 41, no. 5, pp. 1323–1330, Mar. 2019.

[18] D. Jeltsema and J. M. A. Scherpen, "Tuning of passivity-preserving controllers for switched-mode power converters," *IEEE Trans. Autom. Control*, vol. 49, no. 8, pp. 1333–1344, Aug. 2004.

[19] H. Rodriguez, R. Ortega, G. Escobar, and N. Barabanov, "A robustly stable output feedback saturated controller for the boost DC-to-DC converter," *Syst. Control Lett.*, vol. 40, no. 1, pp. 1–8, May 2000.

[20] C.-Y. Chan, "Simplified parallel-damped passivity-based controllers for DC–DC power converters," *Automatica*, vol. 44, no. 11, pp. 2977–2980, Nov. 2008.

[21] Y. I. Son and I. H. Kim, "Complementary PID controller to passivity-based nonlinear control of boost converters with inductor resistance," *IEEE Trans. Control Syst. Technol.*, vol. 20, no. 3, pp. 826–834, May 2012.

[22] J. Alvarez-Ramirez and G. Espinosa-Pérez, "Stability of current-mode control for dc-dc power converters," *Syst. Control Lett.*, vol. 45, no. 2, pp. 113–119, 2002.

[23] H. Rodriguez, R. Ortega, and G. Escobar, "A new family of energy-based non-linear controllers for switched power converters," in *Proc. ISIE . IEEE Int. Symp. Ind. Electron.*, 2001, pp. 723–727.

[24] H. K. Khalil and J. W. Grizzle, *Nonlinear Systems*, Vol. 3. Upper Saddle River, NJ, USA: Prentice-Hall, 2002.

[25] G. Tao, "A simple alternative to the barbalat lemma," *IEEE Trans. Autom. Control*, vol. 42, no. 5, p. 698, May 1997.

[26] S. Aranovskiy, A. Bobtsov, R. Ortega, and A. Pyrkin, "Performance enhancement of parameter estimators via dynamic regressor extension and mixing," *IEEE Trans. Autom. Control*, vol. 62, no. 7, pp. 3546–3550, Jul. 2017.

[27] M. Tavan, K. Sabahi, and A. Hajizadeh, "A filtered transformation via dynamic matrix to state and parameter estimation for a class of second order systems," *Int. J. Control, Autom. Syst.*, vol. 17, no. 9, pp. 2242–2251, Sep. 2019.